THE ARCHIVE OF MECHANICAL ENGINEERING

Vol. LII 2005 Number 2

Key words: *hydrodynamics, gasdynamics, oil consumption, elastic contact, surface roughness, piston engines*

*ANDRZEJ WOLFF**), *JANUSZ PIECHNA***)

NUMERICAL SIMULATION OF PISTON RING PACK OPERATION IN THE CASE OF MIXED LUBRICATION

The motion of a ring pack on a thin oil film covering a cylinder liner has been analysed. In contrast to the previous paper [8], which considered only hydrodynamic phenomena, in the present paper a mixed lubrication case is also taken into account. Equations describing the mixed lubrication problem based on the empirical mathematical model formulated in works of Patir, Cheng [5], [6] and Greenwood, Trip [2] have been combined and used in this paper.

Results of numerical simulations of this phenomenon have been presented. The model of ring motion considered takes the following phenomena into account: hydrodynamic and contact forces, spring and gas forces and the local motion of each ring in piston grooves. Differences between the motion of the ring on a thick and thin oil film are analysed and discussed.

NOMENCLATURE

A_c – real area of contact per unit circumference,
E_1, E_2 – modulus of elasticity of cylinder liner and ring,
E – composite elastic modulus,
F_A – friction force per unit circumference due to asperity contact,
F_{Fr} – friction force per unit circumference due to viscous shear,
F_{Hyd} – radial hydrodynamic force per unit circumference,
h – nominal oil film thickness,

*) *Warsaw University of Technology, Faculty of Transport, ul. Koszykowa 75, 00-662 Warsaw, Poland; E-mail: wolff@it.pw.edu.pl*

**) *Warsaw University of Technology, Institute of Aeronautics and Applied Mechanics, ul. Nowowiejska 24, 00-665 Warsaw, Poland; E-mail: jpie@meil.pw.edu.pl*

h_T – local oil film thickness $h_T = h + \delta_1 + \delta_2$,
$\bar{h}_T$ – average separation (gap between the ring face and cylinder liner),
p – pressure,
$\bar{p}$ – mean hydrodynamic pressure,
t – time,
u – piston velocity / axial velocity of moving ring face,
$V_{r1} = (\sigma_1/\sigma)^2$ – variance ratio of liner surface roughness,
$V_{r2} = (\sigma_2/\sigma)^2 = 1 - V_{r1}$ – variance ratio of ring surface roughness,
W_A – radial force per unit circumference due to asperity contact,
x – spatial coordinate,
β – asperity radius of curvature,
η – asperity density,
γ – surface roughness anisotropy parameter,
ρ – density of lubricant,
μ – oil dynamic viscosity,
δ_1, δ_2 – roughness amplitudes (asperity heights) of surfaces measured from their mean levels,
δ – composite (combined) roughness (asperity height): $\delta = \delta_1 + \delta_2$,
σ_1, σ_2 – standard deviations of asperity height distributions: δ_1, δ_2,
$\sigma = \sqrt{\sigma_1^2 + \sigma_2^2}$ – composite root-mean – square (RMS) roughness,
τ_A – shear stress in surface film arising from asperity interactions,
τ_0 – shear strength constant,
τ_1, τ_2 – hydrodynamic components of shear stress,
ν_1, ν_2 – Poisson's ratio of cylinder liner and ring,
ϕ_{fp}, ϕ_{fs} – shear stress factors,
ϕ_s – shear flow factor,
ϕ_x – pressure flow factor,
Φ_s, Φ_{fs} – factor defined in text.

1. Introduction

Piston rings, principally used to seal the gap between the piston and cylinder to prevent loss of combustion gases, are important components in internal combustion engines.

To cover a wide range of functions like: sealing, lubrication and heat transfer, rings are constructed in packs. The typical pack consists of rings of different lip geometry, stiffness and thickness. In recent years, the number of rings in ring packs has generally been reduced to 3. A pack as analysed consists of a barrel faced upper compression ring, a scraper second compression ring and a twin rail oil control ring.

This study presents the results of numerical simulation of a four-stroke engine with a piston ring pack operating at high temperature. In contrast to previous investigations [8] new physical phenomena related to the existence of thin oil films are taken into account. An integrated methodology has been applied which takes into account coupled effects between the ring radial and axial motion, a conjunction of gas flow in the inter-ring regions, mixed lubrication phenomena at the ring-liner interface, oil transport, wear load and oil consumption.

The main objective of the present investigation is to provide better predictions for the ring minimum film thickness, friction, power loss, oil consumption due to scraping, inter-ring gas dynamics and ring motion in cases of full and mixed lubrication.

In the previous paper [8] the motion of a ring pack on an oil film covering the cylinder liner was considered. The previous analysis was limited to the case of full lubrication and thick oil films. It was assumed that the oil film thickness is greater than the mean value of the cylinder liner surface roughness. Such conditions exist only in the case of relatively low working temperatures and high oil viscosities.

The use of modern oil of low viscosity, working at a high temperature causes the existence of a very thin oil film thickness comparable to the value of the liner surface roughness. In such conditions, the possibility of direct contact between the ring and cylinder liner surface exists.

2. Technical problems

To prevent leakage of combustion gases through the gap, which is necessary between the cylinder liner and piston, rings located in grooves in the piston wall are commonly used. To further reduce the friction between the cylinder liner and ring lips, a thin layer of oil between them is applied.

At high temperatures during the modern engine operation the viscosity of sealing oil is low, and the resulting oil film thickness becomes comparable to the liner and ring surface roughness. During the piston motion, there exist some periods of very low motion velocity when the hydrodynamic forces are also low and the probability of direct contact between the slowly moving ring and cylinder liner also exists.

On the other hand, depending on the ring and groove geometry, combustion gases create radial gas dynamic forces acting to increase the ring diameter and also to increase the probability of its contact with the cylinder liner.

Transferring these technical problems into the physical domain means that one has to recognise several physical phenomena required in a ring pack motion model.

3. Physical problems

Many physical phenomena are associated with ring pack operation, such as:

- hydrodynamic action in the gap between the ring land and cylinder liner,
- inter-ring gas dynamics for blow-by and blow-back behaviour,
- mixed lubrication at the ring face-liner conjunction for friction considerations,
- oil transport for distribution of lubricant along the liner,
- liner temperature influence on the oil viscosity,
- non-Newtonian phenomena associated with shear stresses typical for modern synthetic oils.

The motion of two different fluids has to be considered. At first, the rings slide on a thin layer of oil. Independently, the flow of exhaust gases through crevices among the piston, rings and cylinder liner exists. Both flows are in conjunction. The radial motion of the ring in piston grooves changes the ring end gap, which is mainly responsible for the blow-by value. An exhaust gas leakage influences the temporary variation of the pressure acting on the inner ring surfaces closing the loop of dependencies by influencing the radial ring motion.

It can be assumed that, generally, gas forces are almost independent of hydrodynamic forces. However, hydrodynamic forces strongly depend on gas forces.

If the roughness of surfaces is taken into account, in a given phase of the piston motion the gap between the cylinder liner and the ring lip is so small that it is necessary to consider the mixed lubrication problem.

Typically a great difference exists between the temperature of the upper and lower part of the cylinder liner. This means the temperature of the oil film also varies along the cylinder liner. Because the oil viscosity strongly depends on the oil temperature, liner temperature seems to be a key factor influencing ring operation.

Modern oils have some non-Newtonian characteristics and typically viscosity depends on the local shear rate. At the present level of the investigation this phenomenon has not yet been taken into account.

3.1. Modes of lubrication

In 1902 Stribeck presented a paper showing the influence of velocities of interacting surfaces and of a load on the friction coefficient for a plain journal bearing. Three lubricant modes can be distinguished: boundary lubrication, mixed lubrication and hydrodynamic or elasto-hydrodynamic lubrication. These lubrication modes or regimes can be seen in Fig. 1.

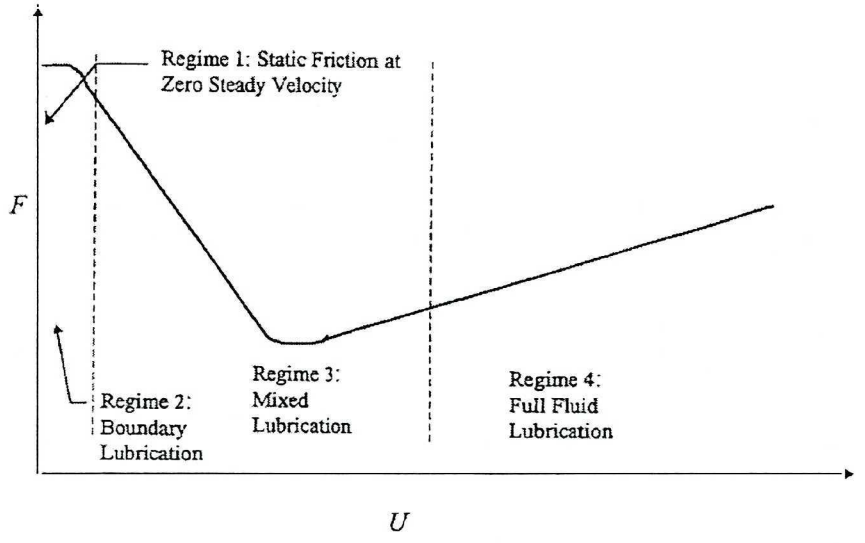

Fig. 1. Stribeck curve – friction force F versus steady velocity U

At high motion velocities, the surfaces are fully separated by an oil film due to a pressure build-up. In this case, the hydrodynamic lubrication in a variable shape gap takes place. When the velocity decreases, the hydrodynamic pressure becomes lower and the asperities of both surfaces begin to touch, and a part of the load is carried by contact forces. As a result, an increase in the coefficient of friction is observed. The friction in this mode, which is called mixed lubrication, is controlled by interacting asperities as well as by oil between the surfaces. As the velocity continues to decrease or the ring load increases, the hydrodynamic action decreases and more asperities are in contact. When a full load is carried by the asperities, the friction phenomenon is controlled by shearing of the boundary layers, which are usually present on solid bodies. In this regime, which is called boundary lubrication, the friction coefficient is nearly independent of the load and surface velocity. These three modes together form the Stribeck curve.

An example of a Stribeck curve is shown in Fig. 1. On the vertical axis of the Stribeck curve the friction coefficient is plotted as a function of moving surface velocity. The piston ring pack of an internal combustion engine moves with variable velocity and load. In reverse points, the axial velocity is very low, but due to the squeeze effect, the radial velocity increases, and the load is partially carried by the hydrodynamic pressure. Therefore, the rings operate in hydrodynamic and mixed regimes of lubrication.

Even a temporary direct contact of the ring surface and cylinder liner has a strong influence on the wear of rings and cylinder liner. Also the geometric

profile of the ring surface and the roughness profile of both surfaces change due to direct contact and resulting wear.

4. Mathematical model

The physical phenomena discussed above can be presented in the form of mathematical relations.

4.1. Hydrodynamic

The equation in the form presented can be used for simulation of the flow in the gap between the ring and cylinder liner.

$$\frac{\partial}{\partial x}\left(\frac{h^3}{\mu}\frac{\partial p}{\partial x}\right) = \underbrace{6u\frac{\partial h}{\partial x}}_{wedge} + \underbrace{12\frac{\partial h}{\partial t}}_{squeeze} \tag{1}$$

This form of Reynolds equation was used in previous piston ring lubrication simulations [8] considering full lubrication cases. The more advanced hydrodynamic analysis of sealing rings invariably predicts very thin oil films comparable to, or less than, typical surface roughness of the ring and liner. The above form of the equation is not fully valid in such conditions. It is, therefore, essential to take asperity interaction and mixed lubrication into account.

In the case of mixed lubrication, a different form of Reynolds equation had to be used.

4.2. Mixed lubrication

The mixed lubrication regime is the intermediate zone between the boundary lubrication regime and the elasto-hydrodynamic lubrication regime. In this case, the applied load is partly carried by the interacting asperities and the remaining part by the fluid film. In order to predict the friction force in the lubrication regime, a contact model had to be applied to calculate the load carried by the asperities and to take into account changes in oil flow conditions.

Assuming that both interacting surfaces (the cylinder liner surface and the ring surface) are rough, the semi-empirical mathematical model formulated by Patir, Cheng [5], [6] and Greenwood, Trip [2] have been combined and used in this work.

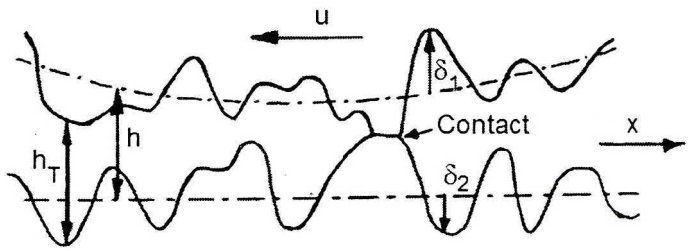

Fig. 2. Surface roughness of a cylinder liner and ring

If h_T is a local oil film thickness defined as:

$$h_T = h + \delta_1 + \delta_2 \tag{2a}$$

the average film thickness (mean gap /separation) is calculated from:

$$\bar{h}_T = E(h_T) = \int_{-h}^{\infty} (h + \delta) f(\delta) d\delta \tag{2b}$$

Assuming the Gaussian distribution of roughness height density, the local value of $f(\delta)$ can be approximated by the following β distribution (see Fig. 3):

$$f(\delta) = \begin{cases} \dfrac{35}{96\sigma}\left[1 - \left(\dfrac{\delta}{3\sigma}\right)^2\right]^3; & |\delta| \le 3\sigma \\ 0 \qquad\qquad\qquad\quad ; & |\delta| > 3\sigma \end{cases} \tag{3a}$$

where the composite root-mean-square (RMS) roughness is:

$$\sigma = \sqrt{\sigma_1^2 + \sigma_2^2} \tag{3b}$$

and

σ_1, σ_2 – standard deviations of asperity height distributions: δ_1, δ_2

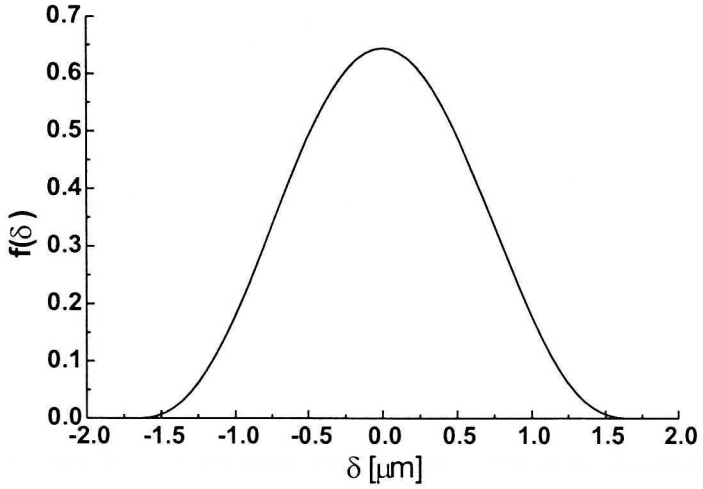

Fig. 3. Applied distribution of roughness height density

Using a relative height of the gap $H = \frac{h}{\sigma}$, one obtains the following mean gap $\bar{h}_T$ in this case:

$$\bar{h}_T = \begin{cases} h & \text{for } H \geq 3 \\ \frac{3\sigma}{256}\left[35 + z\left(128 + z\left(140 + z^2\left(-70 + z^2\left(28 - 5z^2\right)\right)\right)\right)\right] & \text{for } H < 3 \end{cases} \quad (4)$$

where: $z = \frac{H}{3}$

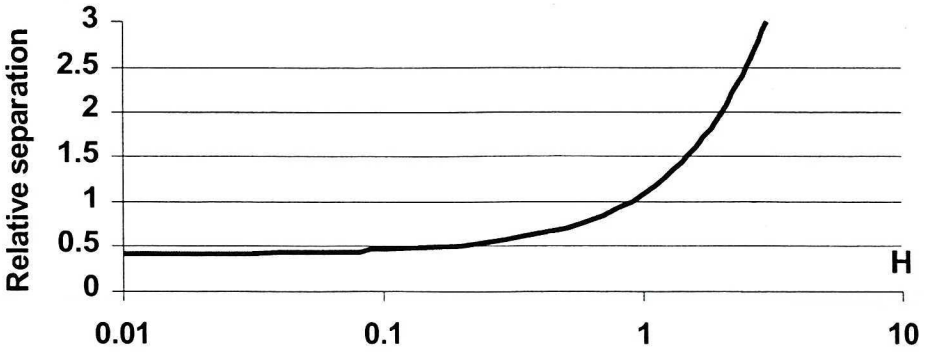

Fig. 4. Relative separation versus relative gap height

The relative separation is defined as $\bar{h}_T/\sigma$. This is presented as a function of the relative gap height in Fig. 4. It can be noticed that even for a very low gap height due to surface roughness the relative separation does not decrease to zero. Tops of summits can interact and elastic contact can occur, but all the time an oil layer exists.

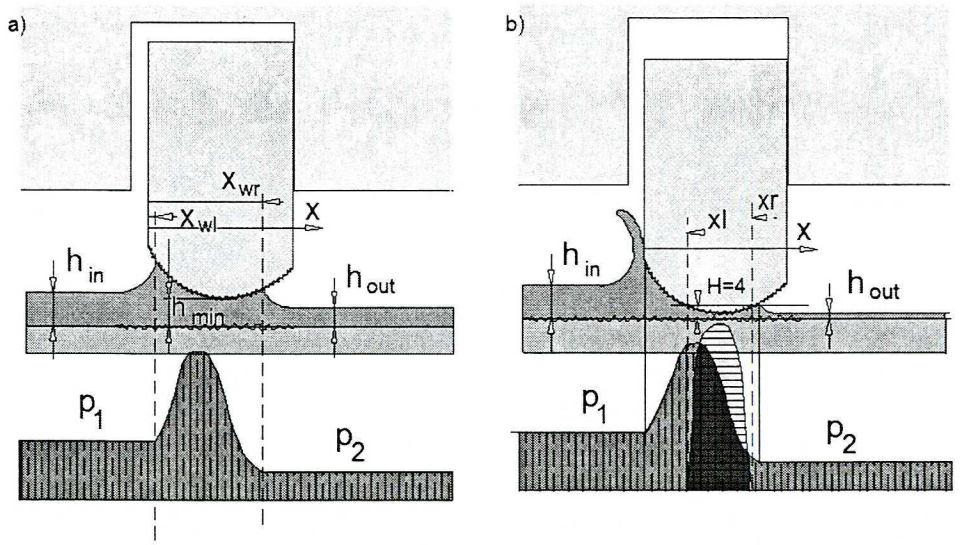

Fig. 5. Flow parameters in the gap between the ring face and cylinder liner in the case of full and mixed lubrication

In Fig. 5 a comparison of basic parameters existing in cases of full and mixed lubrication is presented. If full lubrication exists, only two parameters x_{wl} and x_{wr} defining the range of the wetted area are important. In the case of mixed lubrication, additional parameters x_l and x_r defining the area of surface contact should be taken into account. In the wetted area, hydrodynamic pressure distribution can be noticed (Fig. 5a, 5b), and in the contact area an additional pressure distribution, related to elastic contact between summits of interacting surfaces exists (Fig. 5b).

Concurrently two phenomena exist in the case of mixed lubrication. The first one is oil flow in a complicated area among summits representing the rough surfaces of the cylinder liner and the ring. Having statistical parameters of rough surface geometries, it is possible to use the average form of Reynolds equation (5) for the gap. In this case, a modified gap geometry described by semi-empirical correction coefficients should be applied. The correction coefficients take into account the fact that a part of the gap is occupied by asperities. This permits the calculation of average hydrodynamic pressure. In

a parallel way, the normal and tangential force components exist due to direct contact of extreme parts of both moving surfaces. Therefore, the process can be considered a sum of hydrodynamic action and pure asperity contact action.

4.3. Hydrodynamic action

A one dimensional form of the average Reynolds equation developed by Patir and Cheng [5], [6] has been used to calculate hydrodynamic forces in the case of rough gap surfaces. This equation is applicable to any general roughness structure, and takes the form

$$\frac{\partial}{\partial x}\left(\phi_x \frac{h^3}{12\mu}\frac{dp}{dx}\right) = \frac{U}{2}\frac{dh_T}{dx} + \frac{U}{2}\sigma\frac{d\phi_S}{dx} + \frac{dh_T}{dt} \tag{5}$$

The empirical pressure and shear flow factors, ϕ_x and ϕ_s, enable the average lubricant flow to be related to average quantities such as mean pressure and nominal film thickness.

The pressure flow factor ϕ_x is a correction factor, comparing the mean pressure flow in a rough gap to that of a smooth gap having the same nominal geometry. The factor ϕ_x describes an interaction of opposite surface asperities in the mixed lubrication regime resulting in a decrease in the pressure flow.

This is a function of parameter γ defining a directional pattern, of surface (anisotropy of roughness structure). Many surfaces have directional patterns, which are the result of a manufacturing or wear process. The isotropic surface pattern has the parameter $\gamma = 1$, longitudinally oriented to the motion direction it is defined by $\gamma > 1$, transversely oriented by $\gamma < 1$.

For an anisotropic surface, the flow factors ϕ_x and ϕ_s were evaluated using functions obtained from curve fits of numerical data given in [6]

$$\phi_x(H) = 1 - 0.9\exp(-0.56H) \tag{6}$$

$$\phi_S(H) = V_{r1}\Phi_S(H) - V_{r2}\Phi_S(H) \quad \text{– shear flow factor for combination of two surfaces of the oil gap} \tag{7}$$

where

$$\Phi_S(H) = \begin{pmatrix} 1.899H^{0.98}\exp(-0.92H + 0.05H^2) & H \le 5 \\ 1.126\exp(-0.25H) & H > 5 \end{pmatrix} \quad \text{– shear flow factor for single surface} \tag{8}$$

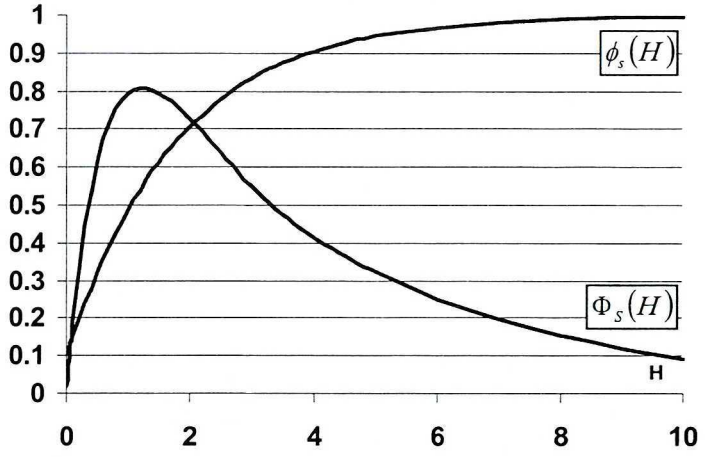

Fig. 6. Variation of ϕ_x and ϕ_s coefficients with H

If two surfaces have statistically identical roughness configurations with the same σ and γ values, then ϕ_s is equal to zero. It means that there is no net flow resulting from the combined effect of sliding and roughness.

Hydrodynamic shear stresses are described by:

$$\tau_1 = \frac{\mu U}{h}(\phi_f + \phi_{fS}) + \phi_{fp}\frac{h}{2}\frac{\partial \bar{p}}{\partial x} \tag{9a}$$

$$\tau_2 = V_{r2}\left\{\left(\phi_{fp}h - \bar{h}_T\right)\frac{\partial \bar{p}}{\partial x} - \frac{2\mu U}{h}\phi_{fS}\right\} \tag{9b}$$

The shear stress factors ϕ_{fp} and ϕ_{fs} may be evaluated using similar empirical relationships to flow factors. In the case of an isotropic surface:

$$\phi_{fp}(H) = 1 - 1.4\exp(-0.66H) \tag{10}$$

is a correction factor for the mean pressure flow component of the shear stress. All values of ϕ_{fp} are less than 1.

$$\phi_{fS}(H) = V_{r1}\Phi_{fS}(H) - V_{r2}\Phi_{fS}(H) \tag{11}$$

The shear flow factor arises from the combined effect of roughness and sliding, a combination of two surfaces brought together
where

$$\Phi_{fS}(H) = 11.1H^{2.31}\exp(-2.38H + 0.11H^2) \tag{12}$$

is a shear flow factor associated with a single surface.

The term ϕ_f arises from averaging the sliding velocity component of the shear stress, and is given by

$$\phi_f = h\left\langle \frac{1}{h_T} \right\rangle \tag{13}$$

The singularity at contact points where $\bar{h}_T = 0$ is overcome by assuming that at some very small film thicknesses the hydrodynamic shear stress no longer exists, and asperity contact has occurred.

Thus

$$\phi_f = h \int_{-h+\varepsilon}^{\infty} \frac{f(\delta)}{(h + \delta)} d\delta \tag{14}$$

where $\varepsilon = \dfrac{\sigma}{100}$ arbitrarily chosen parameter.

The integration of this equation for any given frequency density of roughness heights yields the following numerical relationships

$$\phi_f = \begin{cases} \dfrac{35}{32} z\left\{(1 - z^2)^3 \ln\left(\dfrac{z+1}{\varepsilon^*}\right) + \dfrac{1}{60}[-55 + z\{132 + z(345 + z[-160 + z\{-405 + z(60 + 147z)\}])\}]\right\} & H \le 3 \\ \dfrac{35}{32z}\left[(1 - z^2)^3 \ln\left(\dfrac{z+1}{z-1}\right) + \dfrac{z}{15}(66 + z^2(30z^2 - 80))\right] & H > 3 \end{cases} \tag{15}$$

where $z = \dfrac{H}{3}$; $\varepsilon^* = \dfrac{\varepsilon}{3\sigma}$

The possibility of very large shear stresses which are a consequence of Newton's law of viscosity is prevented by defining a switch function

$$\text{if } \tau(x) > \tau_A(x) \text{ then } \tau(x) = \tau_A(x) \tag{16}$$

where $\tau_A = \tau_0 + \alpha p$ is the shear strength of the surface film. It means that the hydrodynamic shear stress no longer exists and asperity contact has occurred and dominates.

The Reynolds equation can be solved, resulting in a hydrodynamic pressure distribution.

4.4. Asperity interaction and elastic contact model

When pressure is applied to a surface, this surface is deformed. The range of the deformation is strongly determined by the elasticity modulus E of the surface.

The combined elasticity modulus is defined as:

$$E' = \left(\frac{1 - \nu_1^2}{E_1} + \frac{1 - \nu_2^2}{E_2} \right)^{-1} \tag{17}$$

with elastic modules E_1, E_2 and Poisson's ratios ν_1, ν_2 of surface 1 and 2, respectively.

One of the most frequently used elastic contact models is the Greenwood and Tripp [2] model. The authors give a general theory of contact between two rough plane surfaces. In their model, a large number η of asperities (η per m^2) is assumed to be distributed on both contacting surfaces. The average radius of the asperities is β and the height distribution of the surface, $f(\delta)$, as well as that of the summits, $f_s(\delta)$, is assumed to be Gaussian i.e.:

$$f_s(\delta) = \frac{1}{\sigma_s \sqrt{2\pi}} e^{-\frac{\delta^2}{2\sigma_s^2}} \tag{18}$$

where: δ – roughness amplitude (asperity height)

The standard deviation of the summit's height distribution is σ_s and that of the surface height distribution is σ.

The model of asperity interaction developed by Greenwood and Tripp [2] is used in this analysis.

The asperity contact force per unit circumference is given by

$$W_A = 16\sqrt{\frac{2}{15}}\pi(\eta\beta\sigma)^2 E' \sqrt{\left(\frac{\sigma}{\beta}\right)} \int_{x_l}^{x_r} F_{5/2}\left(\frac{h}{\sigma}\right) dx, \tag{19}$$

and the real area of contact per unit circumference by

$$A_c = \pi^2(\eta\beta\sigma)^2 \int_{x_l}^{x_r} F_2\left(\frac{h}{\sigma}\right) dx \tag{20}$$

where the integration limits x_l and x_r define a continuous interval, $x_l \le x \le x_r$ in which $\frac{h}{\sigma} \le 4$

η – asperity density

β – asperity radius of curvature

$\sigma = \sqrt{\sigma_1^2 + \sigma_2^2}$ – composite roughness

The functions F_n have the following form

$$F_2(H) = \begin{cases} 0.44839 \cdot 10^{-4} \exp\left(6.9422097 \ln(4-H) - 0.158491(\ln(4-H))^2\right) & \text{for } H < 4 \\ 0 & \text{for } H \ge 4 \end{cases} \tag{21}$$

$$F_{\frac{5}{2}}(H) = \begin{cases} 0.408827 \cdot 10^{-4} \exp\left(6.803378 \ln(4-H) + 0.09882754(\ln(4-H))^2\right) & \text{for } H < 4 \\ 0 & \text{for } H \ge 4 \end{cases} \tag{22}$$

where: $H = \frac{h}{\sigma}$

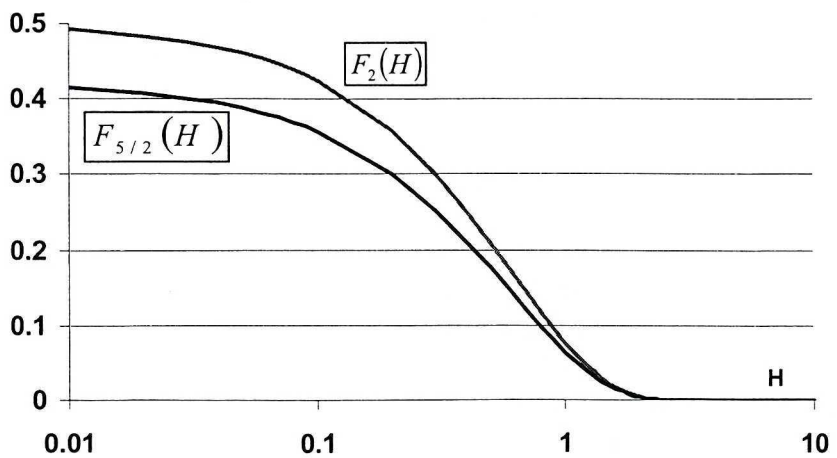

Fig. 7. The variation of $F_2(H)$ and $F_{5/2}$ (H) coefficients with H

The friction forces arising from asperity interaction were calculated by assuming that the shear strength of the surface film was given by

$$\tau_A = \tau_0 + \alpha p \tag{23}$$

so that the integration over the real area of contact gave

$$F_A = \tau_0 A_c + \alpha W_A \tag{24}$$

The constants: $\tau_0 = 2 \cdot 10^6$ $[Pa]$ and $\alpha = 0.08$.

4.5. Viscosity as a function of the liner temperature

The viscosity of the oil used for lubrication is a key factor influencing oil film thickness. Heavy load engines have a relatively high temperature of oil film and due to that a relatively low oil viscosity. This explains the very thin oil film left by the periodically moving ring pack.

In the analysis presented, it was assumed that the oil film temperature is equal to the liner temperature.

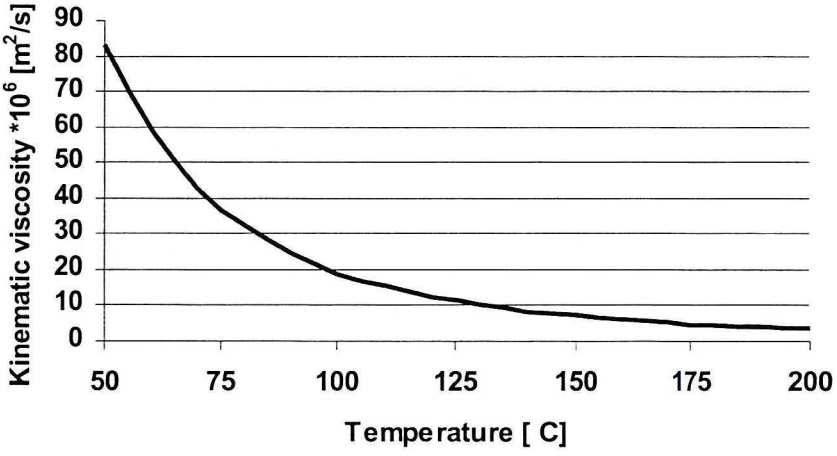

Fig. 8. Oil viscosity versus oil temperature

The variation of oil viscosity with temperature is determined by the commonly used Vogel equation:

$$\mu_0(T) = k \exp\left(\frac{\theta_1}{\theta_2 + T}\right) \tag{25}$$

where: $k = 0.0352\, cSt$

$\theta_1 = 1658.88$°C

$\theta_2 = 163.54$°C for the SA-10W50A multigrade oil

and temperature T [°C].

4.6. The geometry of the ring lip

The profile of the sealing ring is described by

$$h(x) = h_{\min} + \frac{(x - off)^2}{2R} \quad \text{for} \quad 0 < x < d \tag{29}$$

where: $h_{\min}$ – minimal gap height
d – ring width
R – ring surface radius
off – distance of the gap minimal height from the left ring edge

A schematic geometry of the ring pack investigated in the analysis presented is shown in Fig. 10 and 11. The ring pack consists of a compression ring, a scraper ring and an oil ring with two lips. The compression and the scraper ring have asymmetric profiles. The details are given in Table 1.

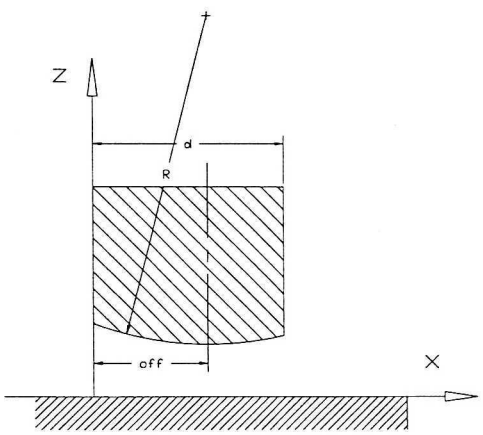

Fig. 9. Definition of the ring lip geometry

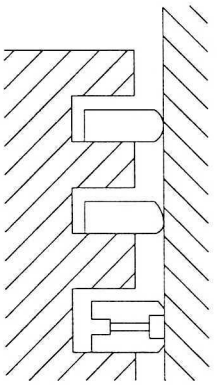

Fig. 10. Typical ring pack in an automotive engine

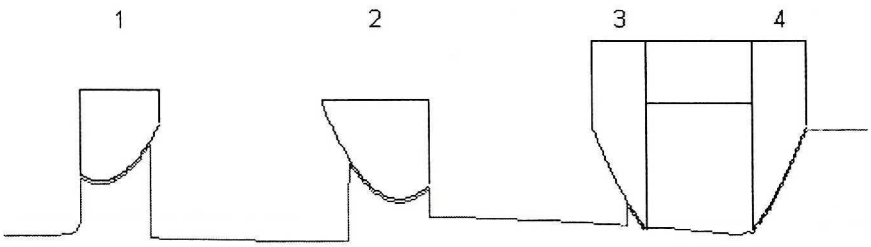

Fig. 11. Ring pack geometry under consideration (1 – compression ring, 2 – scraper ring, 3 – upper lip of the oil ring and 4 – lower lip of the oil ring); the continuous line represents the hypothetical oil film surface

Table. 1

Ring 1:	
Ring width	$B_1 = 1.48$ mm
Offset of the ring profile	$O_{ff1} = 0.37$ mm
Surface radius	$R_1 = 180$ mm
Area of the ring compensation gap (gas flow)	$A_1 = 0.014$ mm^2
Ring elastic tension force (per unit circumference)	$F_{SP1} = 375$ N/m
Ring 2:	
Ring width	$B_2 = 1.98$ mm
Offset of the ring profile	$O_{ff2} = 1.43$ mm
Surface radius	$R_2 = 180$ mm
Area of the ring compensation gap (gas flow)	$A_2 = 0.012$ mm^2
Ring elastic tension force (per unit circumference)	$F_{SP2} = 350$ N/m
Ring 3 (with 2 lands):	
Total ring width	$B_3 = 4.00$ mm
Width of the upper ring land	$B_{U3} = 1$ mm
Width of the lower ring land	$B_{L3} = 1$ mm
Offset of the ring profile	$O_{ff3} = 2$ mm
Surface radius	$R_3 = 244$ mm
Area of the ring compensation gap (gas flow)	$A_3 = 0.012$ mm^2
Ring elastic tension force and spring force (per unit circumference)	$F_{SP3} = 1545$ N/m
Main engine parameters:	
Cylinder diameter	$D_C = 80$ mm
Piston diameter	$D_P = 79.92$ mm
Piston stroke	$S = 79.5$ mm
Lenth of connecting rod	$l = 160$ mm
Engine rotational speed	$n = 3400$ obr/min
Lubrication parameters:	
Growth velocity of the oil film thickness due to oil fog condensation on the cylinder liner under the ring pack	$V_{fog} = 800$ μm/s
Decrease velocity of the oil film thickness in combustion chamber due to evaporation	$V_{evap} = 10$ μm/s
Oil density	$\rho = 900$ kg/m^3

4.7. Boundary conditions

To preserve the solution of the Reynolds equation (1), it is necessary to describe the boundary conditions. It was possible to formulate different boundary conditions [7], but after the consideration of possibilities available, the following way was chosen.

The upstream boundary condition states that the pressure is equal to the gas pressure. The down-stream boundary states that the pressure is equal to the gas pressure and the pressure gradient is equal to zero. Details were presented in the previous paper [8].

4.8. Gas flows

From pressure variation measurements or numerical simulation of the physical process taking place inside the cylinder during the full cycle of the single cylinder operation, the pressure over the first sealing ring is known. The pressure among all the rings can be calculated assuming the isentropic process of expansion and compression inside the volumes among the rings. Due to the relatively high pressure differences between the volumes considered, the gas dynamic equation including critical and subcritical flows in orifices connecting volumes had to be used.

The variation of pressure inside the area filled by gas between rings was determined from the energy equation. The inner energy inside a gas volume depends on the difference between the energy delivered from the area containing a gas of higher pressure and the energy transferred to the area containing a gas of lower pressure. Details of the calculation procedure were presented in the previous paper [8].

4.9. Friction force and power loss

The friction force acting on the ring can be calculated by the following relationship:

$$F(t) = \int_A (\tau + \tau_A) dA \tag{30}$$

The power loss including the loss due to squeeze motion is calculated by

$$P(t) = u(t) \cdot F(t) + F_{hydr} \cdot v_{squeeze} \tag{31}$$

4.10. Oil motion

The motion of each ring also generates the motion of the oil in an oil film. Some rings scrape the oil and accumulate it in front of the ring. The accumulated oil is transported and distributed over the cylinder liner. In the areas of starved flow, the thickness of oil film becomes constant. In the model presented, the oil flow is calculated from the following equation:

$$\bar{q}(x) = -\phi_x \frac{h^3}{12\mu} \frac{\partial \bar{p}}{\partial x} + \frac{u}{2} \bar{h}_T + \frac{u\sigma}{2} \phi_s \tag{32}$$

The term $\frac{u\sigma}{2}\phi_s$ in the equation (32) describes the correction due to the roughness of the gap surfaces.

5. Numerical model

The numerical solution is based on the implicit scheme described in the previous paper [8]. The discretized Reynolds equation with proper boundary conditions forms a tri-diagonal matrix and can be effectively solved in each time step.

A general solution of the ring motion problem was obtained in the following (iterative) way. Assuming that the minimal gap between the ring and cylinder liner h_{min} is known, the vertical velocity (or squeeze velocity) $v_{squeeze}$ is predicted, the hydrodynamic and roughness contact pressure distributions are calculated, and the hydrodynamic force F_{hydr} and contact force W_A estimated and compared with the sum of the gas force F_{gas} and ring elastic tension force F_{spring}.

The radial forces are balanced for each ring, including the following forces:

- hydrodynamic force F_{hydr},
- ring face-liner contact force W_A,
- gas force on unlubricated ring face sections F_{gas},
- installed tension force F_{spring}.

Depending on the difference between the force required and the force calculated, a correction of the vertical velocity is prescribed and a new calculation performed. The iterations are continued until the desired force equilibrium accuracy is reached.

$$F_{hydr}(h_{\min}, v_{squeeze}) + W_A(h_{\min}) \approx F_{spring} + F_{gas} \tag{33}$$

6. Variation of wetted and contact area

In the case of starved lubrication, the main problem is to calculate the position of the left and right ends ($\mathbf{x}_{\mathbf{left}}$ and $\mathbf{x}_{\mathbf{right}}$) of the wetted part of the ring surface (see Fig. 5a). Taking into account the position of maximum pressure and the velocity of the squeeze, the motion of the wetted area boundary is calculated from the continuity equation.

In the case of fully flooded lubrication, it is assumed that a part of the oil film is accumulated in front of the ring lip or moved away by the ring.

It is also assumed that on one side of the ring system the cylinder surface is in the oil fog area. Due to adsorption, the oil film thickness increases with a known velocity. On the opposite side of the ring pack, evaporation of the oil film is assumed.

It is also assumed that gas pressure existing on the left or right side of the ring acts on the back side of the ring, depending on the direction of piston motion.

The definition of the roughness contact area is much simpler than the definition of the wetted area, because in this case the additional parameters x_l and x_r (Fig. 5b) that define the surface contact area boundaries are dependent only on the nominal height of the gap. It was arbitrarily assumed that contact exists only if the value of h/σ is lower than 4. The nominal local gap value of 4σ defines the position of contact boundaries (parameters x_l and x_r).

7. Oil consumption

Oil left on the cylinder liner and not protected by the piston can evaporate at the cycle phase corresponding to the maximum cylinder volume. On the other hand, on the cylinder surface opened to the crankcase an oil fog can be condensed and absorbed. The presented model takes into account these phenomena. A simple model of the constant evaporation velocity and condensation velocity proportional to the exposition time was adopted and used. The motion of a ring pack depends on all existing physical phenomena: ring shapes, oil film thickness, pressure distribution, piston velocity, oil temperature, the oil scraped, transported and distributed along the cylinder liner.

The model of oil consumption due to evaporation is based on the oil film thickness distribution on the liner and the ring pack motion corresponding to the phase when it is exposed to high temperature combustion chamber gas. This happens during the down stroke of the piston, and the amount of oil is dependent on lubrication conditions.

During the up-stroke, the scraping effect of the top ring is responsible for oil accumulation at the leading edge and partial redistribution on the liner.

A fraction of this oil is discharged into the combustion chamber due to inertia effects at the top dead centre.

The model presented utilises the oil-fog scheme of oil film renovation. It assumes that under the piston an oil fog forms from very small uniformly distributed oil droplets. During the up-stroke, a part of the liner oil film is rebuilt by adhesion of these oil droplets.

On the other side of the piston (in the cylinder chamber), oil evaporation is taken into account.

The motion of the ring pack generally scrapes the main part of the added oil in the direction of crankcase and redistributes the rest of oil on the liner.

8. Results of calculation

An automotive internal combustion engine works where a wide range of loads and the resulting thermal conditions exist. In the paper presented, two characteristic thermal states of engine operation were analysed and compared. It was assumed that the first characteristic engine load state is engine warm-up, when the cylinder liner temperature is low. The second characteristic engine state corresponds to the nominal thermal load, when the liner temperature is much higher.

Two calculations have been performed. The first one assumed that the oil temperature equals 93°C. Under this assumption, the oil film is thick enough in comparison with the mean value of the surface roughness. Therefore, the surfaces of rings and cylinder liner can be treated as smooth surfaces. The second calculation is done under the assumption that oil temperature equals 200°C. In this case, the possibility of mixed lubrication is expected and taken into account.

The main parameters of the rough structure of the liner and ring surface are presented in table 2.

Table 2.

Surface data	Value
Asperity density	$\eta = 1 \cdot 10^6$ [m^{-2}]
Asperity radius of curvature	$\beta = 0.2$ [μm]
RMS roughness of cylinder surface	$\sigma_1 = 0.4$ [μm]
RMS roughness of rings surface	$\sigma_2 = 0.4$ [μm]
Elastic modulus of cylinder liner	$E_1 = 2.06 \cdot 10^{11}$ [N/m^2]
Elastic modulus of rings	$E_2 = 2.06 \cdot 10^{11}$ [N/m^2]
Poisson's ratio of cylinder liner	$\nu_{P1} = 0.3$
Poisson's ratio of rings	$\nu_{P2} = 0.3$

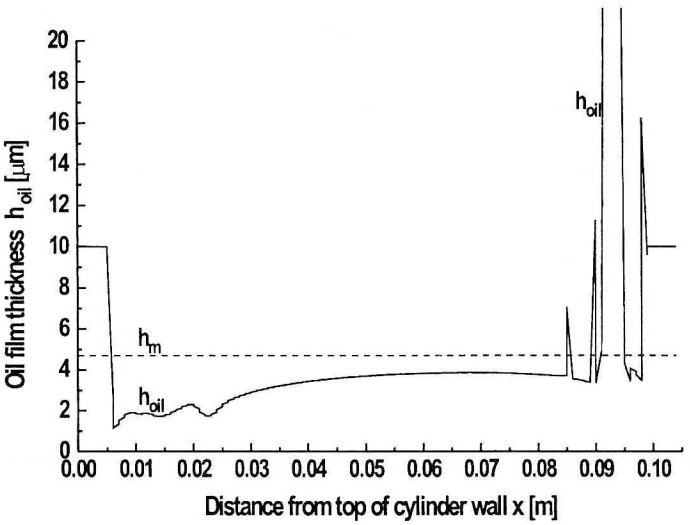

Fig. 12. Variation of the oil film thickness left by the ring pack. Calculation results for smooth surfaces and oil temperature of 93°C

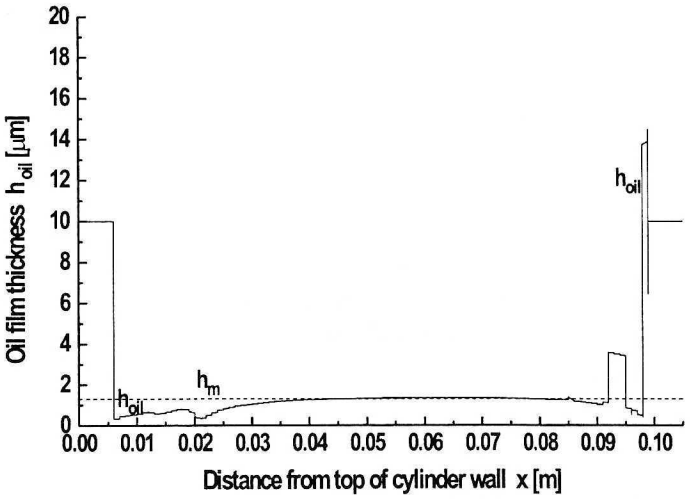

Fig. 13. Variation of the oil film thickness left by the ring pack. Calculation results for rough surfaces and oil temperature of 200°C

An important calculation result is the oil film thickness distribution on the liner after a few cycles of ring pack operation. The motion of the ring pack scraping and distributing oil on the cylinder liner leaves the oil film profile shown in Fig. 12 and 13 after a few cycles of operation. Fig. 12 contains the results for low liner temperature, and by comparison Fig. 13 shows the results for the higher liner temperature. The low oil film thickness near the top dead

centre and peaks of accumulated oil near the leading ring lips can be clearly seen. The difference of the oil film thickness along the area of ring pack motion is very important. In the case of lower liner temperature, the minimum film thickness is higher than 1 μm, in contrary to the case of higher temperature, where the oil film thickness decreases to 0.2–0.3 μm. It can be noticed that RMS roughness of both interacting surfaces equals 0.4 μm.

The very low local film thickness values, in both cases, near the top dead centre can be explained by the existence of high gas pressure values existing in this area during the compression and working strokes of engine operation. In Fig. 14, gas pressure variations in spaces among the rings are presented. The pressures existing in these areas act on the back surfaces of rings pushing them into the liner direction. Most of all, phases of high pressure acting on the compression ring can be noticed.

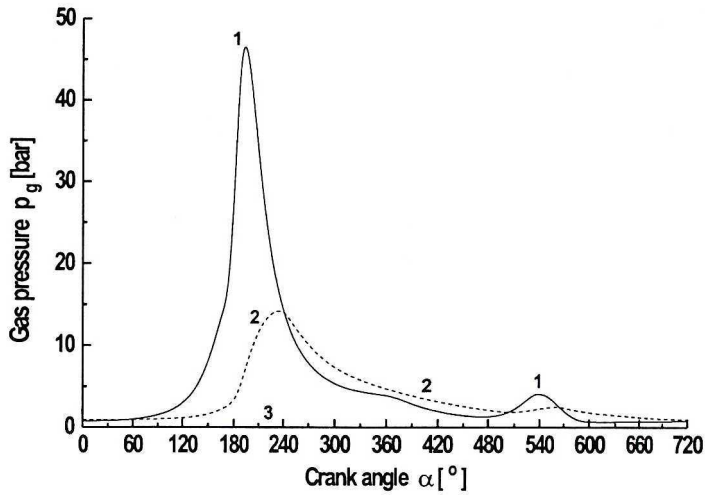

Fig. 14. Variation of the gas pressure acting on piston rings as a function of crankshaft rotation (1 – compression ring, 2 – scraper ring, 3 – oil ring)

Gas and ring elastic tensing forces must be compensated by hydrodynamic forces generated in the ring-liner gap and, additionally, in the mixed lubrication cases expected, by elastic contact forces.

In Fig. 15 variations in radial components of elastic contact forces are visible. These forces occur in the case of a high temperature of the cylinder liner near top and bottom dead centre. The values of elastic contact forces are 3–4 times lower than hydrodynamic forces acting on rings.

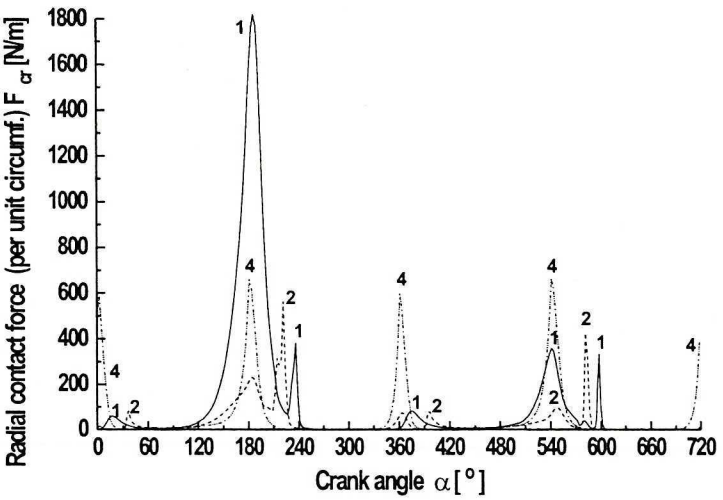

Fig. 15. Variation of radial components of contact forces for each piston ring as a function of crankshaft rotation (1 – compression ring, 2 – scraper ring, 3 – upper lip of the oil ring and 4 – lower lip of the oil ring). Calculation results for rough surfaces and oil temperature of 200°C

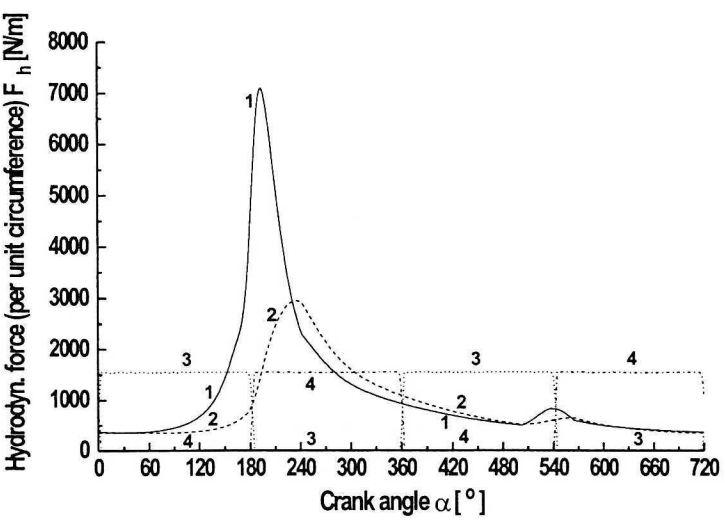

Fig. 16. Variation of hydrodynamic forces generated by each piston ring as a function of crankshaft rotation (1 – compression ring, 2 – scraper ring, 3 – upper lip of the oil ring and 4 – lower lip of the oil ring). Calculation results for smooth surfaces and oil temperature of 93°C

Figs. 16 and 17 present the hydrodynamic forces for each ring land necessary for the compensation of both gas pressure and radial force resulting from ring elastic tensing. Fig. 16 contains results for the low liner temperature, and by comparison Fig. 17 shows the results for the higher liner temperature. The similar form of all curves is characteristic, but slightly lower

force values can be observed in the case of higher liner temperature. Correlating results presented in Fig 16 and 17 with the data showed in Fig.12 and 13 one can conclude that force differences are results of some load transfer from the hydrodynamic forces to the elastic contact forces.

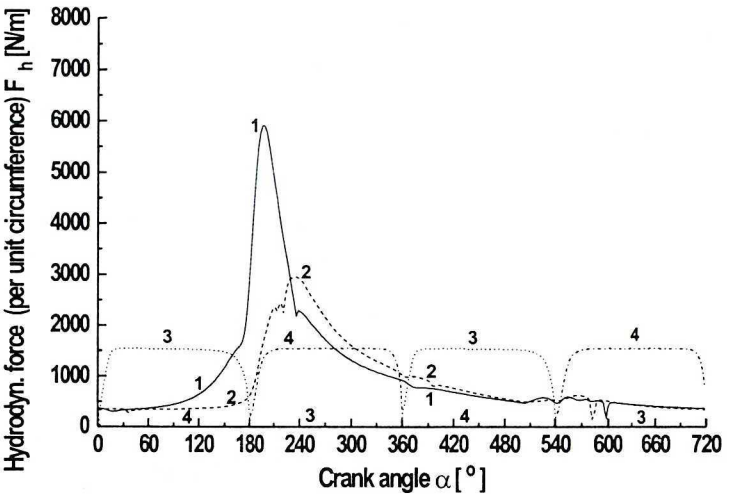

Fig. 17. Variation of hydrodynamic forces generated by each piston ring as a function of crankshaft rotation (1 – compression ring, 2 – scraper ring, 3 – upper lip of the oil ring and 4 – lower lip of the oil ring). Calculation results for rough surfaces and oil temperature of 200°C

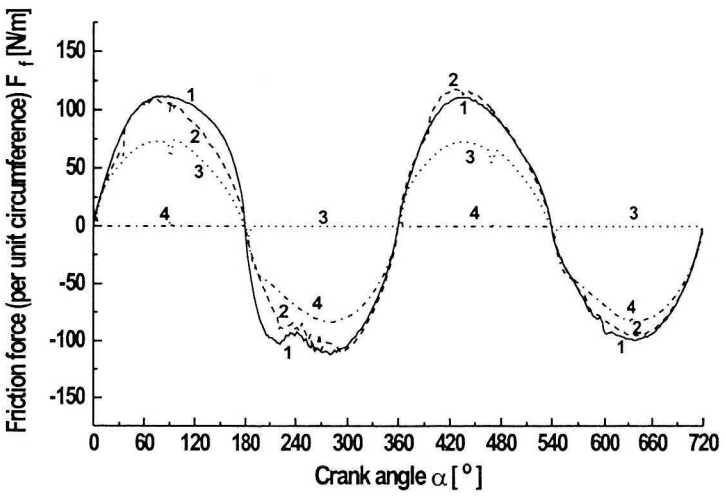

Fig. 18. Variation of unit tangential forces acting on each piston ring as a function of crankshaft rotation (1 – compression ring, 2 – scraper ring, 3 – upper lip of the oil ring and 4 – lower lip of the oil ring). Calculation results for smooth surfaces and oil temperature of 93°C

A similar tendency can be expected for the variation of tangential components of forces (friction forces) acting on the rings (see Fig. 18 and Fig. 19). At low oil temperature only, the hydrodynamic friction force could be noticed (Fig. 18), but at high oil temperature the additional tangential component of elastic contact force had to be included (Fig. 20).

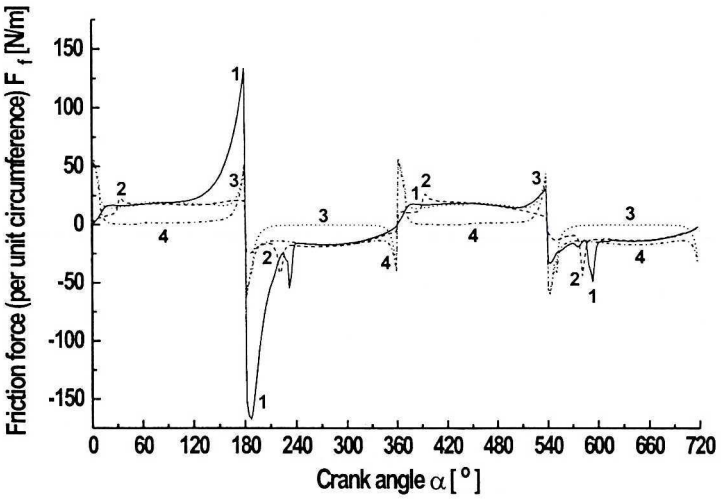

Fig. 19. Variation of unit tangential forces acting on each piston ring as a function of crankshaft rotation (1 – compression ring, 2 – scraper ring, 3 – upper lip of the oil ring and 4 – lower lip of the oil ring). Calculation results for rough surfaces and oil temperature of 200°C

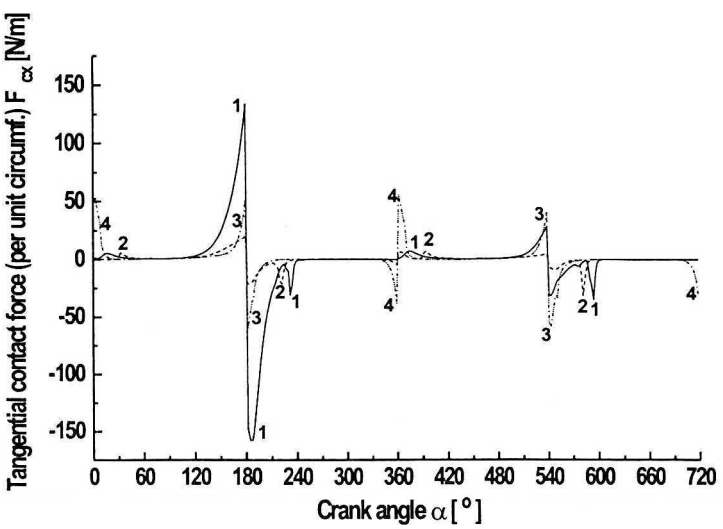

Fig. 20. Variation of tangential components of contact forces for each piston ring as a function of crankshaft rotation (1 – compression ring, 2 – scraper ring, 3 – upper lip of the oil ring and 4 – lower lip of the oil ring). Calculation results for rough surfaces and oil temperature of 200°C

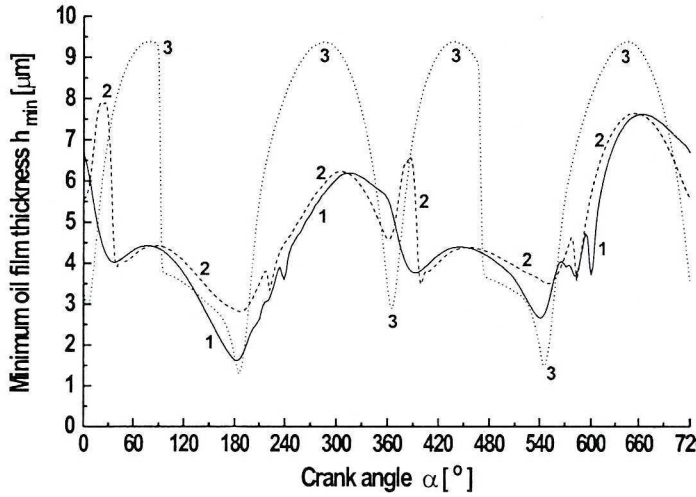

Fig. 21. Variation of ring land-liner distance as a function of crankshaft rotation (1 – compression ring, 2 – scraper ring, 3 – oil ring). Calculation results for smooth surfaces and oil temperature of 93°C

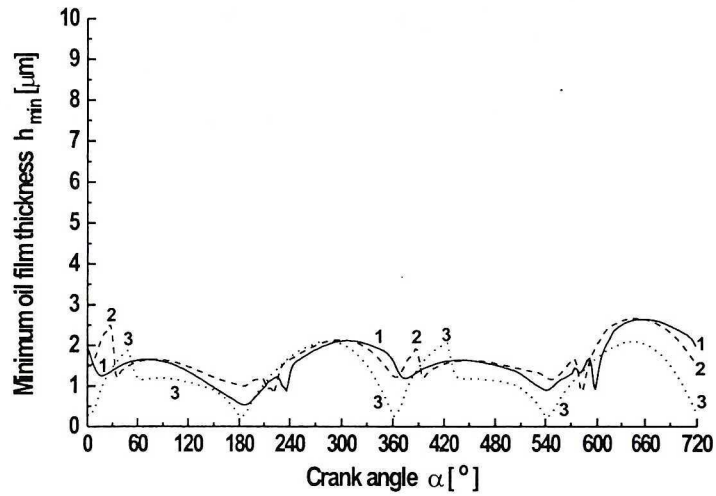

Fig. 22. Variation of ring land-liner distance as a function of crankshaft rotation (1 – compression ring, 2 – scraper ring, 3 – oil ring). Calculation results for rough surfaces and oil temperature of 200°C

Figs. 21 and 22 present a variation of the ring land-liner distance as a function of crankshaft rotation for low and high liner temperature, respectively. In the case of lower liner temperature (Fig. 21), the top ring has lower minimum film thickness values during the expansion stroke due to a higher gas load (groove pressure) compared to any other part of the cycle. The second ring, having a scraper face profile, has lower minimum film

thickness values during down-strokes than up-strokes. There is not much difference between the minimum film thickness values for the oil ring rails during the up-stroke and down-stroke. This can be attributed to the fact that the oil ring is quite insensitive to the low groove pressure acting behind it. In addition, the high value of installed spring force causes a significant scraping, and therefore promotes a substantial oil accumulation at the leading edges even in the case of a relatively low oil supply. As a result, the minimum film thickness behaviour for the oil ring shows a low sensitivity to oil supply conditions. All the curves in the case of higher oil temperature have completely different forms. The variation amplitude of the ring land-liner distance and its minimum values are lower.

Detailed information about the scraping capabilities of all rings is presented in Fig. 23 and Fig. 24. In both figures, volumes of oil accumulated by each ring are shown and compared. The oil transportation along the liner has the same character (Fig. 23 and 24), but the volumes of oil scraped by the first and second ring during up-strokes are quite different. In the case of mixed lubrication (Fig. 24), mainly due to a lower mean oil film thickness, the oil volumes scraped are certainly much lower than the volumes shown in Fig. 23. In contrast, the oil volumes scraped by the lower lip of the third ring (the oil ring) during down-strokes are almost the same, because the velocity of oil film thickness growth due to oil fog condensation on the cylinder liner is the same in both cases.

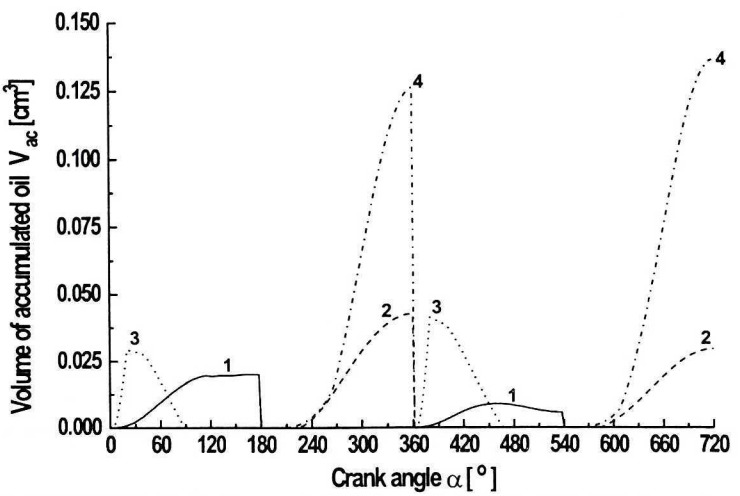

Fig. 23. Volume of oil accumulated by each ring as a function of crankshaft rotation (1 – compression ring, 2 – scraper ring, 3 – upper lip of the oil ring and 4 – lower lip of the oil ring). Calculation results for smooth surfaces and oil temperature of 93°C

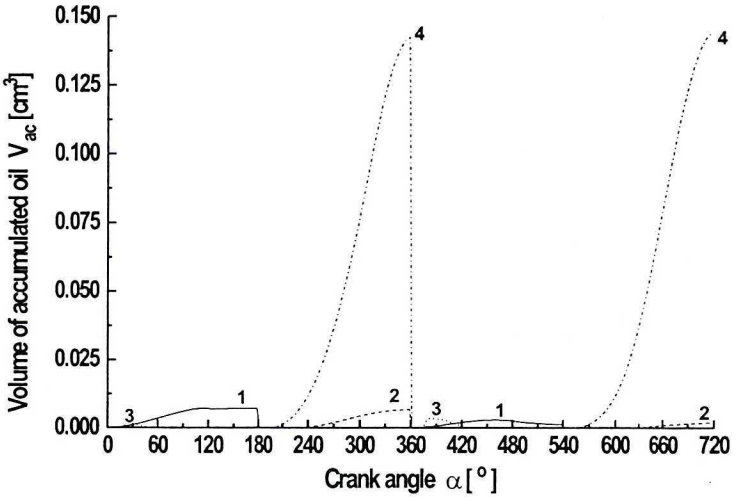

Fig. 24. Volume of oil accumulated by each ring as a function of crankshaft rotation (1 – compression ring, 2 – scraper ring, 3 – upper lip of the oil ring and 4 – lower lip of the oil ring). Calculation results for rough surfaces and oil temperature of 200°C

Oil film thickness, piston velocity, ring elastic tensing and parameters of surface roughness cause variation in the ring land wetted area and also the elastic contact area in the case of mixed lubrication. Ring lands are very often only partially flooded in the phases of high piston velocity. In contrast, they are fully flooded in the phases of low piston velocity.

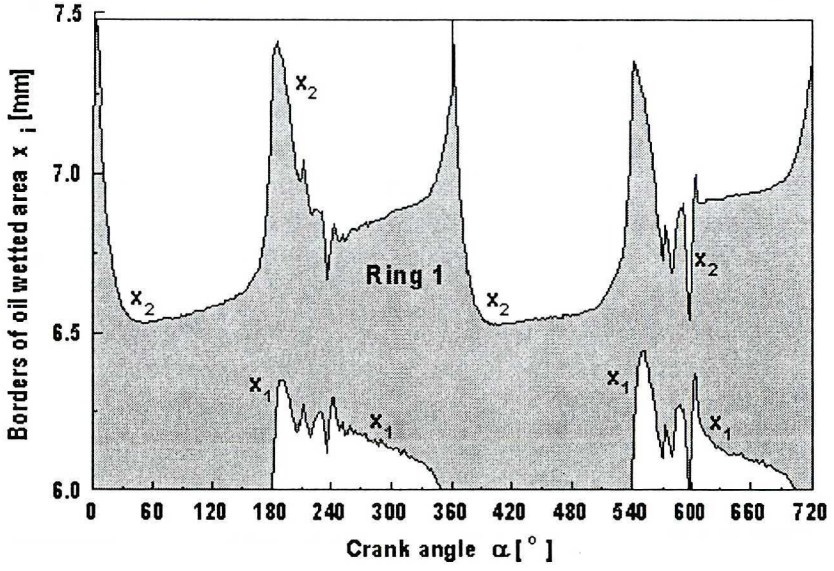

Fig. 25. Oil wetted area of the compression ring as a function of crankshaft rotation, x_1, x_2 – upper and lower boundaries. Calculation results for smooth surfaces and oil temperature of 93°C

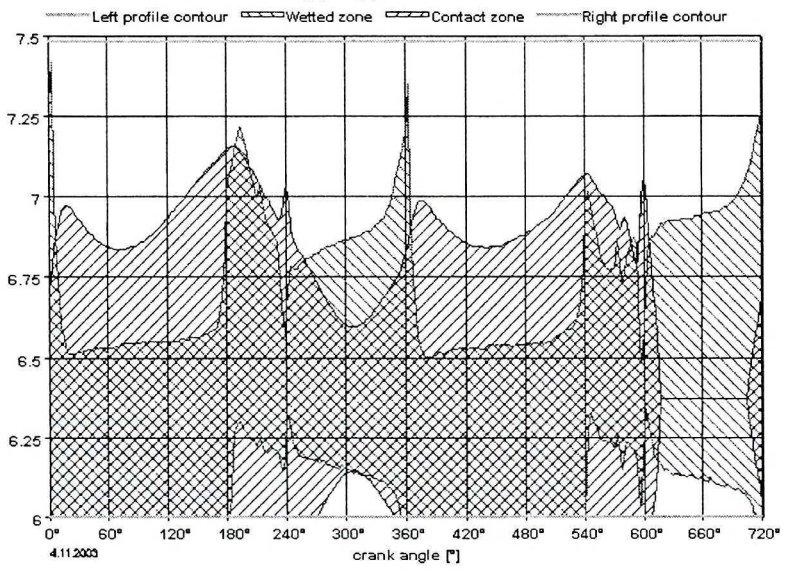

Fig. 26. Oil wetted area and contact zone of the compression ring as a function of crankshaft rotation, x_1, x_2 – upper and lower boundaries. Calculation results for rough surfaces and oil temperature of 200°C

For comparison purposes, variations in the wetted areas of the compression ring are presented in Fig. 25 and 26. Additionally, in Fig. 26 corresponding to the case of high liner temperature and mixed lubrication, boundaries of the contact area are shown. Due to very low oil film thickness and arbitrary defined contact limit ($h/\sigma = 4$), an arrival of elastic contact area outside the oil wetted area is noticeable. In both cases, the full lubrication (Fig. 25) and mixed lubrication (Fig. 26), the shapes of the wetted areas look very similar.

A similar tendency can be observed in Fig. 27 and 28 showing variations in the wetted area and the contact area for the scraper ring. For this ring, the wetted area is visibly reduced in the case of mixed lubrication (Fig. 28).

The two-land oil ring shows the same pattern (Fig. 29 and 30) of wetted area distribution in both cases. It can be seen that depending on the direction of the piston motion, only the leading ring land is wetted with starvation on the trailing land. The full lubrication case is presented in Fig. 29, and the mixed lubrication case in Fig. 30. In addition, a small area of contact in the central ring part is observed in the case of mixed lubrication.

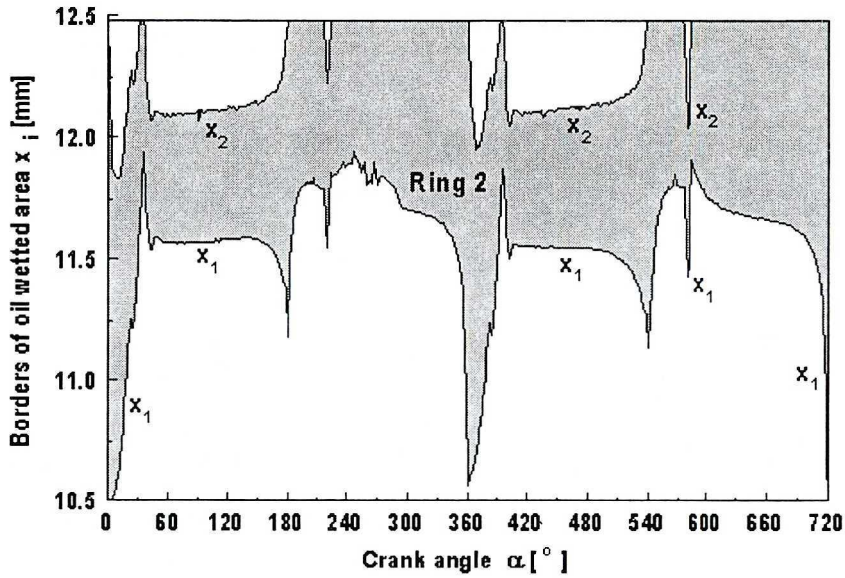

Fig. 27. Oil wetted area of scraper ring as a function of crankshaft rotation, x_1, x_2 – upper and lower boundaries. Calculation results for smooth surfaces and oil temperature of 93°C

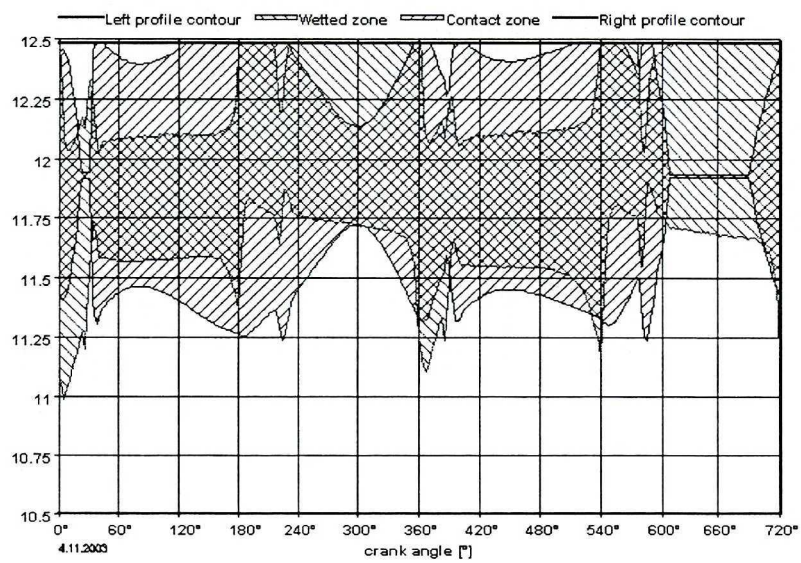

Fig. 28. Oil wetted area and contact zone of the scraper ring as a function of crankshaft rotation, x_1, x_2 – upper and lower boundaries. Calculation results for rough surfaces and oil temperature of 200°C

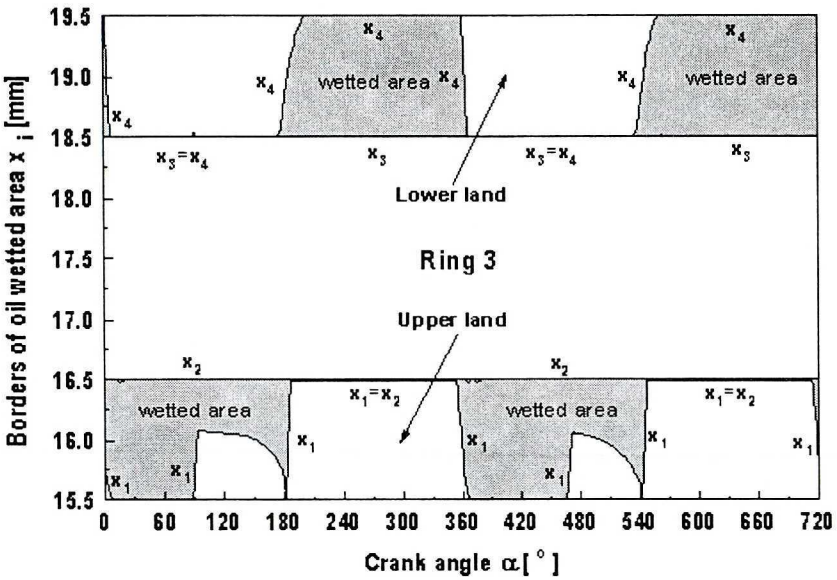

Fig. 29. Oil wetted area of oil ring lands as a function of crankshaft rotation; x_1, x_2 – upper and lower boundaries of the upper land; x_3, x_4 – upper and lower boundaries of the lower land. Calculation results for smooth surfaces and oil temperature of 93°C

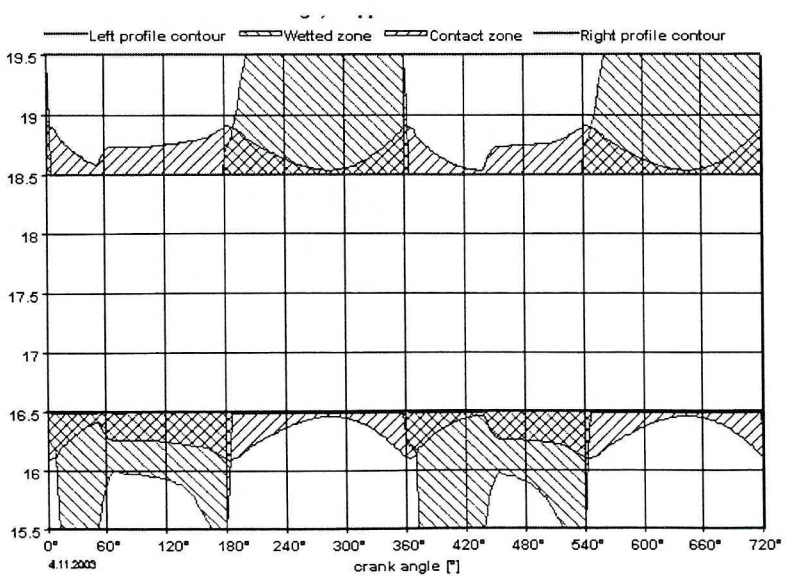

Fig. 30. Oil wetted areas and contact zones of oil ring lands as a function of crankshaft rotation; x_1, x_2 – upper and lower boundaries of the upper land; x_3, x_4 – upper and lower boundaries of the lower land. Calculation results for rough surfaces and oil temperature of 200°C

9. Conclusions

In the paper the authors present, a numerical adaptation of the mixed lubrication empirical mathematical model formulated by Patir, Cheng [5], [6] and by Greenwood, Trip [2] to the simulation of the lubrication of the automotive ring pack. Solutions of the same ring pack working at low and high oil temperature have been compared. A high oil viscosity in the first case generated a thick oil film. In this case, the conventional Reynolds equation can be applied without any corrections. The relatively strong reduction of oil viscosity due to an increase in oil film temperature reduces radically the temporary oil film thickness to values comparable to the liner and ring surface roughness. In this case is necessary to use a more complicated model of the flow in the ring-liner gap. It consists of a modified Reynolds equation containing some correcting parameters and a model of elastic contact of two rough surfaces. In that way, a mixed lubrication with areas of elastic contact of interacting surfaces was analysed. It seems that the mixed lubrication model should be the basic model used in automotive ring pack analysis.

The oil temperature has a very strong influence on oil viscosity and therefore on the lubrication conditions of the ring pack. A high temperature of the cylinder liner surface reduces the oil viscosity used for the lubrication. It is a key factor influencing oil film thickness. The low oil viscosity is the main reason for the very thin oil film left by the periodically moving ring pack. The reduction of the oil viscosity on one hand radically reduces friction losses (3–4 times in analysed case), but on the other hand, due to low oil film thickness, increases the possibility of the existence of the contact of rough surface structures. This effect temporarily increases friction forces (up to 6 times), and causes the cylinder liner and rings wear.

In the preent work, the rough surface structure has been assumed to be constant and equal along the liner and ring length. Taking into account the results of calculations performed, it seems to be necessary to modify this assumption. It has been shown that in some liner areas a direct contact between sliding surfaces exists, which can generate the destruction of part of the rough structure and modify it. It seems to be necessary to use a non-uniform distribution of roughness parameters along the liner. Also it would be possible to correct the ring land shape modified by its surface wear.

Oil viscosity is also dependent on two additional parameters. The first one is local shear rate and the second one is hydrodynamic pressure. Due to very low oil film thickness, the local shear rate can be high enough to stimulate the arrival of non-Newtonian oil properties. In addition, local pressure values existing in the ring-liner gap can significantly change oil viscosity.

The addition of all the factors presented above, which have not yet been included in the numerical code, would probably change some of the global parameters like: the distribution of oil film thickness, friction forces, areas of wetting and elastic contact.

The influence of these factors will be the main topic of the next paper.

Manuscript received by Editorial Board, November 29, 2004;
final version, March 21, 2005.

REFERENCES

[1] Gelinck E.: Mixed Lubrication of Line Contacts, PhD Thesis, University of Twente, 1999.
[2] Greenwood J., Trip J. H.: The contact of Two Nominally Flat Rough Surfaces, Proc Instn Mech Engrs., Vol. 185. 48/71 pp. 625 ÷ 633, 1971.
[3] Liu Q.: Friction in Mixed and Elastohydrodynamic Lubricated Contacts Including Thermal Effects, PhD Thesis, University of Twente, 2002.
[4] Odyck van D. E. A.: Stokes Flow in Thin Films, PhD Thesis, University of Twente, 2001.
[5] Patir N., Cheng H. S.: An Average Flow Model for Determining Effects of Three-Dimensional Roughness on Partial Hydrodynamic Lubrication, Transactions of ASME, Journal of Lubrication Technology, Vol. 100, January 1978.
[6] Patir N., Cheng H. S.: Application of Average Flow Model to Lubrication Between Rough Sliding Surfaces, Transactions of ASME, Journal of Lubrication Technology, Vol. 101, April 1979.
[7] Radcliffe C. D., Dowson D.: Analysis of Friction in a Modern Automotive Piston Ring Pack, Lubricant and Lubrication/ D. Dowson et al. (editors), Elsevier Science B.V., 1995.
[8] Wolff A., Piechna J.: Numerical simulation of piston ring pack operation, The Archive of Mechanical Engineering, Vol. L, Number 3, pp. 303 ÷ 329, 2003.
[9] Yun J. E., Chung Y., Chun S. M., Lee K. Y.: An Application of Simplified Average Reynolds Equation for Mixes Lubrication Analysis of Piston Ring Assembly in an Internal Combustion Engine, SAE Paper 952562, 1996.

Numeryczna symulacja pracy pakietu pierścieni tłokowych w przypadku smarowania mieszanego

Streszczenie

W pracy przedstawiono model ruchu pakietu pierścieni tłokowych przemieszczających się po filmie olejowym o grubości porównywalnej z wysokością chropowatości pierścieni i gładzi cylindrowej. Zaadaptowano model przepływu w szczelinie o chropowatych ściankach Patira i Chenga [5], [6] oraz model elastycznego kontaktu chropowatych powierzchni Greenwooda i Tripa [2]. W modelu uwzględniono siły hydrodynamiczne, siły elastycznego kontaktu i siły sprężystości pierścieni, jak też siły gazowe działające na poszczególne pierścienie. Porównano ruch pierścieni przy niskiej i wysokiej temperaturze powierzchni cylindra, co odpowiada przypadkom pełnego i częściowego smarowania. Pokazano zmiany obszaru zwilżania pierścieni oraz strefy kontaktu, rozkład grubości filmu olejowego, sił działających na pierścienie. Wyniki obliczeń przedstawiono w formie wykresów.